The Development of Arctic Air Masses in Northwest Canada and Their Behavior in a Warming Climate

JESSICA K. TURNER AND JOHN R. GYAKUM

Department of Atmospheric and Oceanic Sciences, McGill University, Montreal, Quebec, Canada

(Manuscript received 18 May 2010, in final form 11 January 2011)

ABSTRACT

Surface observations, soundings, and a thermodynamic budget are used to investigate the formation process of 93 arctic airmass events. The events involve very cold surface temperatures—an average of −42.8°C at Norman Wells, a centrally located station in the formation region—and cooling in the 1000–500-hPa layer. A multistage process for their formation in northwestern Canada is proposed. This process is contrary to the classical conceptualization of extremely shallow, surface formations.

In the first stage of formation, snow falls into a layer of unsaturated air in the lee of the Rocky Mountains, causing sublimational cooling and moistening the subcloud layer. Simultaneously, the midtroposphere is cooled by cloud-top radiation emissions. In the second stage, snowfall abates, the air column dries, and clear-sky surface radiational cooling predominates, augmented by the high emissivity of fresh snow cover. The surface temperature falls very rapidly, up to a maximum of 18°C day^{-1} in one event. In the final stage, after near-surface temperatures fall below the frost point, ice crystals and, nearer the surface, ice fog form. At the end of formation, there is cold-air damming, with a cold pool and anticyclone in the lee of the Rockies, lower pressure in the Gulf of Alaska, and an intense baroclinic zone oriented northwest to southeast along the mountains.

There have been secular changes in the characteristics of the arctic air masses over the period 1948–2008. The surface temperature during the events has become warmer, and the air masses are deeper and moister. The 1000-hPa diabatic cooling during events, which includes latent heat and radiative processes, has decreased by 2.2°C day^{-1}.

1. Introduction

It is well established that the global mean surface temperature has been increasing, at a rate of 0.3°C ± 0.1°C decade^{-1} over the period 1979–2005, as deduced from the Climate Research Unit dataset (Brohan et al. 2006). Nevertheless, this warming has considerable geographic and seasonal variability. It is strongest in the winter season [December–February (DJF)], and the greatest warming region of North America is a band oriented northwest to southeast, stretching from Alaska and the western arctic, to the northern edge of the boreal forest, along the lee of the Rocky Mountains. (Jones and Moberg 2003; Smith and Reynolds 2005; Vose et al. 2005). Northwestern Canada is also known as the primary genesis location for arctic air masses and their associated anticyclones (Zishka and Smith 1980), although there is little scientific literature on the formation of these events. More attention has been paid to what are called cold-air outbreaks, a term generally associated with arctic air masses after they travel into the Midwest and southern United States causing extreme low temperature anomalies. These outbreaks are known to have their genesis in Alaska and the northwestern Canadian arctic (Cellitti et al. 2006; Colucci and Davenport 1987; Dallavalle and Bosart 1975; Konrad and Colucci 1989; Walsh et al. 2001).

There is some disagreement over the formation mechanism of these arctic airmass anticyclones. Bodurtha (1952), Colucci and Davenport (1987), and Ioannidou and Yau (2008) found the forcing to be dynamic, associated with strong 500-hPa ridging over western North America and subsequent anticyclonic vorticity advection and subsidence downstream of the ridge. Alternatively, in several modeling studies Curry (1983, 1987) finds the anticyclones to be associated with diabatic

Corresponding author address: Jessica K. Turner, Dept. of Atmospheric and Oceanic Sciences, McGill University, 805 Sherbrooke St. West, Montreal QC H3A 2K6, Canada.
E-mail: jessica.turner@meteo.mcgill.ca

DOI: 10.1175/2011JCLI3855.1

cooling by surface fluxes of outgoing longwave radiation with additional radiative cooling from condensate in the low level of the atmosphere.

The original model of arctic airmass development was presented by Wexler (1936, 1937). He postulated that the cold air was formed at the surface by radiative cooling from a snow-covered ground under clear, windless conditions, creating an intense temperature inversion restricted to a very shallow layer at the surface. However, actual soundings indicated a deeper layer of cooling than could be explained by this model because the subsidence and high stability accompanying the surface cooling restricts the possibility for upward mixing of the cold air. Finding that the Wexler model could not adequately explain the depth of the cold layer observed in soundings, Gotaas and Benson (1965) identified the importance of suspended ice crystals to upper-level cooling, and Curry (1983) later modeled the effect with the introduction of condensate, particularly ice-crystals, in the layer. The study used a one-dimensional model following the trajectory of air over a homogeneous snow surface. In an experiment without moisture, the inversion that formed after 2 weeks of radiative cooling was less than 1000 m deep. The effect of various parameters including turbulent mixing and subsidence was examined. Only with the addition of ice crystals did the inversion rise above 900 hPa. More recently, Emanuel (2009) also used a single-column radiative–convective model, utilizing a tropical sounding, to simulate the formation of arctic air. The rates and depth of cooling in the model were extremely sensitive to the amount of water vapor and clouds. When clouds were allowed to form, they cooled the layers at their top through radiation while warming the lower layers, both radiatively and with latent heat release.

Although the absolute moisture content of the arctic is low, the relative humidity can be high, so clouds, ice crystals, and ice fogs are common. Ice crystals occur in the arctic year-round throughout a deep layer, exceeding 3 km in some instances (Curry et al. 1990). They are formed by ice nucleation at temperatures typically below −20°C and in the absence of clouds. Ice crystals radiate longwave energy thereby cooling the layer in which they are embedded. Closer to the surface, ice fogs under surface inversions are also common. The top of an ice fog layer will cool radiatively, whereas downwelling radiation will inhibit surface cooling.

A case study of the intense anticyclone and subsequent cold-air outbreak in the winter of 1989 by Tan and Curry (1993) used the complete height tendency equation to show that the event was not a typical cold-core anticyclone since it was primarily forced by negative vorticity and upper-level cold-air advection, rather than diabatic cooling—although diabatic cooling did play a small role. However, it is known both through observations (Portis et al. 2006; Walsh et al. 2001) and modeling studies (Curry 1983; Emanuel 2009; Vavrus 2007) that snow cover is a requirement for the formation of these air masses. Dallavalle and Bosart (1975) examined two polar anticyclones and found them to be a mixed type, supported by both upstream ridging and radiative cooling. In the context of climate change, less effective radiative cooling due to increased greenhouse gas concentrations could change the intensity of the low-level temperature inversion and surface temperature anomalies. Graversen et al. (2008) showed that the vertical structure of the warming in the cold season arctic is greatest at the surface, implying less intense temperature inversions and therefore less intense arctic air masses, as measured by surface temperature. However, Turner and Gyakum (2010) found that, although the mean temperature was increasing in northwestern Canada, the intensity of the coldest temperatures relative to a 30-yr running mean was not changing significantly.

In summary, northwestern Canada has been warming during the winter season since the midtwentieth century, and it is during the winter season that arctic air masses—responsible for the most extreme minimum temperatures in the region—are formed. Given the possible links between regional climate change in northwestern Canada and arctic airmass formation, and the lack of literature on their formation, the purpose of this paper is to investigate arctic airmass formation mechanisms and possible secular changes in their behavior. We will perform the investigation primarily through a synoptic and thermodynamic analysis of 93 such events.

2. Data and methodology

a. Data

Daily minimum surface temperatures at 175 stations across Canada were provided by the Meteorological Service of Canada. This dataset has been corrected for nonclimatic inhomogeneities from sources such as changes in instrumentation or location (Vincent et al. 2002). The start date of observations in this dataset varies from station to station, from the late 1890s in the southeast of the country to the 1950s at some northern stations. Figure 1 shows the location of the stations and the least squares linear trend in winter (DJF) temperature for the period 1950–2007 at the stations. In the figure, the region of greatest warming, stretching from northwest to southeast to the east of the Rocky Mountains, can be seen. This is also a formation region of arctic air masses.

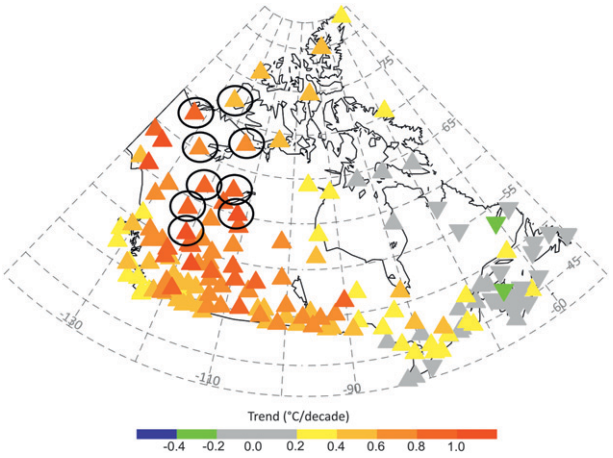

FIG. 1. Least squares linear regression trend in the winter (DJF) mean surface temperature from 1948 to 2007 at 175 stations across Canada. Stations used in this paper for the determination of cold events are circled.

Ten stations in the maximum-warming region with good-quality long-term temperature records were chosen and are circled in Fig. 1. Most of the stations are at low elevation with the exception of Grande Prairie at 669 m. During the winter months, these high-latitude stations have extremely short days, and several of the most northern stations have 24-h darkness at the winter solstice. Table 1 provides the name, latitude, longitude, altitude, length of daylight during the winter solstice, and magnitude of the warming trend at the 10 stations chosen for this study, arranged from most northern to most southern in latitude. These 10 stations mark out an area of roughly 1 million square kilometers with a range of 17 degrees of latitude. The land cover is snow-covered tundra, effectively radiating as a blackbody with very high emissivity.

To examine the formation processes of the air masses responsible for the cold events we will calculate the thermodynamic budgets from the National Centers for Environmental Prediction (NCEP)–National Center for Atmospheric Research (NCAR) global reanalysis (Kalnay et al. 1996). The advantage of this product is its availability beginning in 1948. However, the complicated topography of the western mountains, an important component of the atmospheric dynamics in the region under study here, is not fully resolved by its relatively coarse resolution. The quality of the data is poorer before 1979 because of the lack of satellite data. However, the thermodynamic budgets will be presented at Norman Wells, a station involved in nearly every event and located centrally in the Mackenzie River basin. There have been soundings at this station since July 1955, which have been assimilated into the reanalysis. The reanalysis and upper-air observations are in good agreement at this location.

Another dataset used in this study is the hourly weather observations from the Environment Canada National Climate Data and Information Archive. These observations exist for most of the time period under consideration; the Sachs Harbour record begins at a later date of 1955. Finally, there are soundings at Norman Wells beginning in 1955. Results for Norman Wells will be presented as a proxy for behavior over the entire region.

b. Methodology

Owing to the large differences in latitude and local climate at the individual stations, cold events are defined using temperature anomalies. Cold events are defined as three or more consecutive days of minimum temperature anomalies below one monthly standard deviation at an individual station for at least 5 of the 10 stations. Since there is also a trend toward warmer temperatures at these stations, events defined by anomalies relative to a stationary mean will be clustered at the beginning of the time series. For example, in their assessment of

TABLE 1. The latitude, longitude, altitude, daylight hours at the winter solstice, and trend in winter (DJF) mean surface temperature from 1948–2007. Stations are listed from most northern to most southern.

Station	Lat (°N)	Lon (°W)	Alt (m)	Min daylight (h)	Trend (°C decade^{-1})
Sachs Harbour	72.0	125.3	86	0	0.8
Inuvik	68.3	133.5	68	0	0.9
Kugluktuk	67.8	115.1	23	0	0.5
Norman Wells	65.3	126.8	74	4	0.8
Yellowknife	62.5	114.4	206	5	0.9
Fort Simpson	61.8	121.2	169	5	0.8
Fort Smith	60.0	112.0	205	6	0.9
Fort Nelson	58.8	122.6	382	6	0.8
Fort McMurray	56.7	111.2	369	7	0.5
Grande Prairie	55.2	118.9	669	7	0.7

TABLE 2. The total number of cold event days; the mean duration of the events ± standard deviation; the longest duration of an event; mean intensity ± standard deviation; and coldest day for the periods 1948–62, 1963–77, 1978–92, and 1993–2007. Intensities and coldest days are normalized by monthly standard deviation (σ) of temperature at a given station where the event takes place, to account for the large differences in latitude between stations in the study region.

	Total (events)	Mean duration (days)	Longest duration (days)	Mean intensity (normalized by σ)	Coldest day (normalized by σ)
1948–62	21	4.5 ± 1.6	7	−1.7 ± 0.1	−3.5
1963–77	29	4.8 ± 2.9	15	−1.6 ± 0.2	−3.6
1978–92	25	5.5 ± 2.9	13	−1.7 ± 0.2	−4.6
1993–2007	18	5.8 ± 3.8	18	−1.7 ± 0.2	−4.3

Canadian cold spells, Shabbar and Bonsal (2003) defined events as three or more consecutive days of temperature anomalies below the 5th percentile, and they found decreasing frequency and intensity of cold events using this definition. For the purposes of this study, we define the daily minimum temperature anomalies relative to a 30-year running mean calculated for each day and station with a 15-day smoothing applied to the daily climatology. At the end of the time series, we use the 1992 daily climatology for subsequent years. Using a running-mean climatology, instead of a long-term mean as in Shabbar and Bonsal (2003), eliminates clustering of cold events in the beginning of the time series due to trends in the mean. Any trends in the intensity or duration will remain. We use the monthly standard deviation in the event definition to avoid clustering of events in January, the most variable month. We can now compare the synoptic and thermodynamic behavior of cold events throughout the time series in isolation from shifts in the mean of the temperature distribution.

This paper focuses on synoptic-scale events. By requiring that at least 5 out of 10 stations report anomalously cold temperatures we are selecting events that impact a large geographic area. Although any 5 of the 10 stations could contribute, in practice, the southern stations were more likely to be involved in events. The percentage of days that a station contributed to an event, from north to south, are as follows: Sachs Harbour, 25%; Inuvik, 50%; Kugluktuk, 26%; Norman Wells, 76%; Fort Simpson, 87%; Yellowknife, 79%; Fort Nelson, 75%; Fort Smith, 86%; Fort McMurray, 84%; and Grande Prairie, 78%.

Ninety-three cold events were identified. Some statistics of the events are given in Table 2 partitioned into four time periods: 1948–62, 1963–77, 1978–92, and 1993–2007. The events are approximately evenly distributed throughout the partitioned periods, although there are fewer in the 1993–2007 period, a consequence of the anomalies in this period calculated relative to the 1992 climatology, during which time there was a strong upward trend in mean temperature. The average duration of an event is between 4 and 6 days. There is no trend in the average intensity of the events, shown in the table as a normalized monthly standard deviation, which is between −1.6 and −1.7. The coldest intensity day is increasing slightly—from −3.5 standard deviations in the 1948–62 period to −4.3 standard deviations during the 1993–2007 period. This is consistent with the findings of Turner and Gyakum (2010), who found that while there are warming trends in the mean temperature of northwest Canada, cold anomalies relative to a running mean are not warming.

The thermodynamic budget will be calculated at the 1000-, 925-, 850-, 700-, 600-, and 500-hPa levels using the thermodynamic equation on a constant pressure surface given by

$$\underset{\text{A}}{\frac{\partial T}{\partial t}} = \underset{\text{B}}{-\mathbf{v}\cdot\nabla_{\text{H}}T} + \underset{\text{C}}{\omega\left(\frac{\alpha}{C_p}-\frac{\partial T}{\partial p}\right)} + \underset{\text{D}}{\frac{1}{C_p}\frac{dQ}{dt}}, \quad (1)$$

where T is the temperature (K), t is time (seconds), $\mathbf{v}$ is the horizontal wind field (m s^{-1}), ∇_H is the horizontal gradient, ω is the vertical wind (hPa^{-1}), α is the specific volume $R'T/p$ where R' is the individual gas constant (287 J kg^{-1} K^{-1}), Cp is the specific heat capacity (1005 J kg^{-1} K^{-1}), p is the pressure (hPa), and dQ/dt is diabatic heating (J kg^{-1} s^{-1}). The time change in temperature at a point (A) is equal to horizontal advection (B) plus the vertical term (adiabatic expansion/compression and vertical advection, C) and the diabatic heating term (D). Diabatic heating includes sensible, latent, and radiative heating processes.

To calculate the terms, finite differences were substituted for derivatives. The daily temperature change term (A) at an NCEP–NCAR grid point is the 24-h temperature difference at 0600 UTC from one day to 0600 UTC the next. This period corresponds most closely to the calendar day in the Rocky Mountain time zone. The total daily horizontal advection term (B) is the sum of four 6-hourly periods of advection. These 6-hourly periods are calculated as the average of the period's two

endpoints' instantaneous advection calculated at the grid point, using the actual wind. The vertical term (C) is also the sum of four 6-hourly periods at the grid point. Additionally, the gridpoint stability $\partial T/\partial p$ is computed as the difference in temperature at the grid point between 1000–925, 1000–850, 925–700, 850–600, 700–500, and 600–400 hPa for the 1000-, 925-, 850-, 700-, 600-, and 500-hPa levels, respectively.

We assume that the atmosphere is unsaturated. This introduces some error in the calculation since surface reports of snow and ice fog during the event indicate saturated layers in the atmosphere. If there is ascent in a saturated atmosphere, then we compute too large a value of cooling in the vertical term. The residual term will be equivalently large with an opposite sign of latent heating associated with saturated large-scale ascent. The magnitude of the error will be small at these temperatures. For example, the difference between saturated and unsaturated ascent starting from −20°C at 850 to 600 hPa is approximately 2°C.

3. Synoptic and thermodynamic characteristics of events

During the formation of arctic air masses, different cooling mechanisms dominate at different heights. To examine the depth of cooling during the events, we compare the daily minimum surface temperature at Norman Wells with 1000–500-hPa thicknesses for the 20 days before and during the event itself. The correlation between the time series of surface temperature and 1000–500-hPa thicknesses will be large and positive if the cooling is a deep-layer phenomenon and will be small or negative if the cooling is restricted to the surface. For most events, there is a high correlation between the surface temperature and the 1000–500-hPa thicknesses, indicating deep-layer cooling. For 69% of events the correlation coefficient is above 0.5, and in 60% of events the correlation is above 0.6. Figure 2 shows the frequency distribution of the correlation, with the portion of the distribution above the 80th percentile (0.8) and below the 20th percentile (0.4) shaded.

We divide the events into the following: deep events—the 80th percentile and greater of thickness/surface temperature correlation; shallow events—20th percentile and less of correlation; and the remainder are considered mixed events. Using this definition, there are 21 deep events, 19 shallow events, and 53 mixed events. The initial cooling at Norman Wells may take place many days before the start of an event as defined by our methodology. Therefore, we define the genesis as the 3 days with the largest least squares linear regression surface-cooling trend at any time in the 20 days before the event itself.

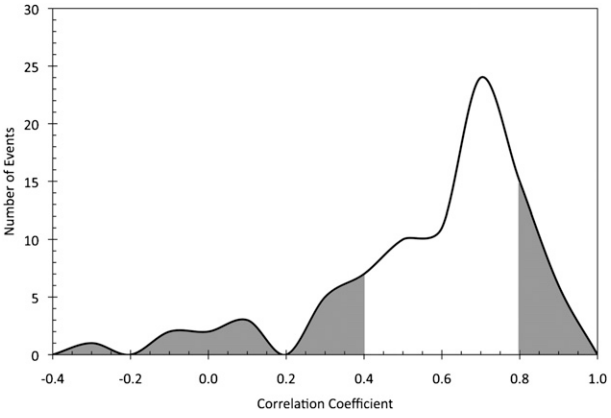

FIG. 2. Frequency distribution of the correlation coefficient between daily minimum surface temperature and 1000–500-hPa thicknesses for the 20 days up to and including an event at Norman Wells. The area below the 20th percentile (0.4) and above the 80th percentile (0.8) is shaded.

The restriction of a formation period to 3 days is better suited to events with rapid cooling—the most common—rather than those that take place over several weeks, but it is applied to all events for consistency.

Figure 3 presents selected examples of daily minimum surface temperature and thickness time series at Norman Wells for a deep, mixed, and shallow event. These examples were chosen from the period for which sounding data exists, based on their representativeness of category type. The event days are shaded. A vertical line marks the genesis. The shaded event days may not necessarily coincide with the lowest temperatures at Norman Wells because of the requirement that 5 out of 10 stations observe anomalously low temperatures; however, Norman Wells is located in the air mass in all 3 examples. Although deep and mixed cases involved cooling processes acting throughout the 1000–500-hPa layer, surface processes are also important. For example, Fig. 3a exhibits a deep-layer cooling, augmented by a surface cooling during the genesis. The shallow case (Fig. 3c) shows the troposphere to be warming during the event, even as the surface temperature cools.

a. Genesis

Figure 4a is the composite 1000–500-hPa thickness and sea level pressure on days 1–3 of genesis for the 53 mixed events. To give an indication of the anomaly magnitudes contained in the composites, contours of 12-hPa standard deviation in sea level pressure (dashed, black) and contours of 14-dam (decameter) standard deviation of thickness (solid, black) are also plotted. Deep and shallow event structures are similar to the mixed events and are omitted for brevity. On day 1, a 1024-hPa anticyclone is present over the western Arctic Ocean

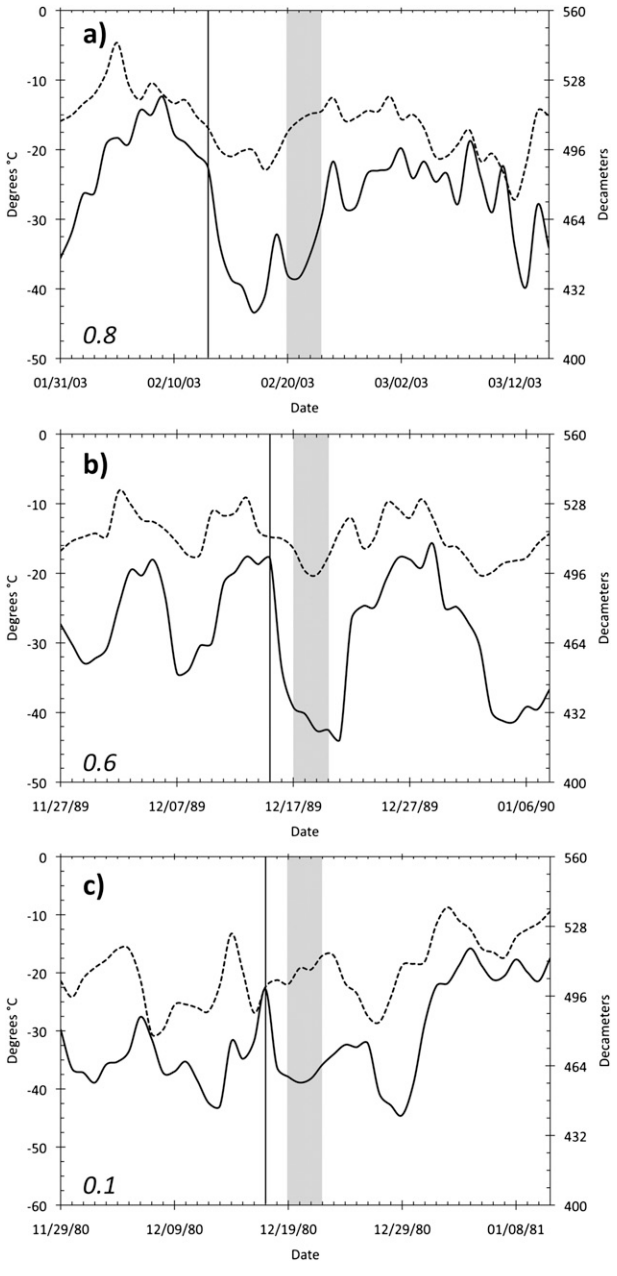

FIG. 3. Time series of daily minimum surface temperature (bold line) and 1000–500-hPa thicknesses (dashed line) at Norman Wells for the 20 days before an event, the event itself, and 20 days after an event for (a) a deep-layer event on 20–23 Feb 2003, (b) a mixed-type event on 17–21 Dec 1989, and (c) a shallow-layer event on 19–21 Dec 1980. The correlation coefficient of the temperature and thickness time series for the period before, and during the event, is given in each example. The event period is shaded. A solid vertical line denotes the start of the genesis period.

embedded in a tongue of high pressure stretching from Siberia into northwestern Canada. The coldest thicknesses in North America exist over the islands of the Canadian northwest. As the genesis progresses, the anticyclone moves southward, into the lee of the Rocky Mountains while the coldest thicknesses build westward. On the last day, a baroclinic zone of temperature and pressure gradient exists along the mountains, with low pressure on the windward side and a closed anticyclone on the lee side, indicative of a cold-air damming circulation (Bell and Bosart 1988).

Figure 4b is the composite 1000–500-hPa thickness and sea level pressure anomalies over the same period as Fig. 4a. From days 1–3, thickness anomalies centered on northwestern Canada fall more than 6 dam, to below −12 dam. The first day, there are high pressure anomalies in the Gulf of Alaska, indicating a weaker than climatology Aleutian low. These anomalies weaken over the Pacific and extend into the continental interior by the last day, with 8-hPa anomalies over northwestern Canada. The cold-air anomalies appear to generate locally, although an air mass moving from a climatological position into northwestern Canada could also explain the progression of anomalies seen in Fig. 4b.

We can quantify to what extent the anomalies in these composites are generated locally and to what extent they are advected from other regions by examining the thermodynamic budget. To assess the relative magnitude of the thermodynamic processes acting during the genesis period, each term in the thermodynamic budget of Eq. (1) was calculated at Norman Wells (located centrally in the region of maximum thickness and pressure anomalies, Fig. 4) and averaged for deep, mixed, and shallow events. Figure 5 shows results for the genesis period. The 1000-hPa level is approximately 100–300 m above the surface so extremely shallow temperature inversions will not be captured in this analysis. It can be seen that the height of maximum cooling over the genesis period is 850 hPa in the mixed and deep cases, with the cooling falling off more rapidly with height above 850 hPa in the mixed cases compared to the deep. In the shallow cases, the height of maximum cooling is 1000 hPa.

There is subsidence warming at the 1000–925-hPa levels throughout the genesis in all cases, indicative of the high pressure in the Northwest Territories (Fig. 4). Ascent, as indicated by cooling in the vertical term, is present above 925 hPa during days 1–2 in the deep and mixed cases, but on day 3 there is subsidence in all levels and event types. Cold-air advection is an important contributor to cooling at the beginning of the genesis period. The geostrophic wind is northerly at this time (Fig. 4) as high pressure enters the region from the north but it becomes weak on day 3 when the air mass becomes well established locally with a close circulation at the surface. The residual term contributes to cooling in all events, especially from 850 hPa and below in the deep and mixed events. Averaged over the entire 1000–500 hPa

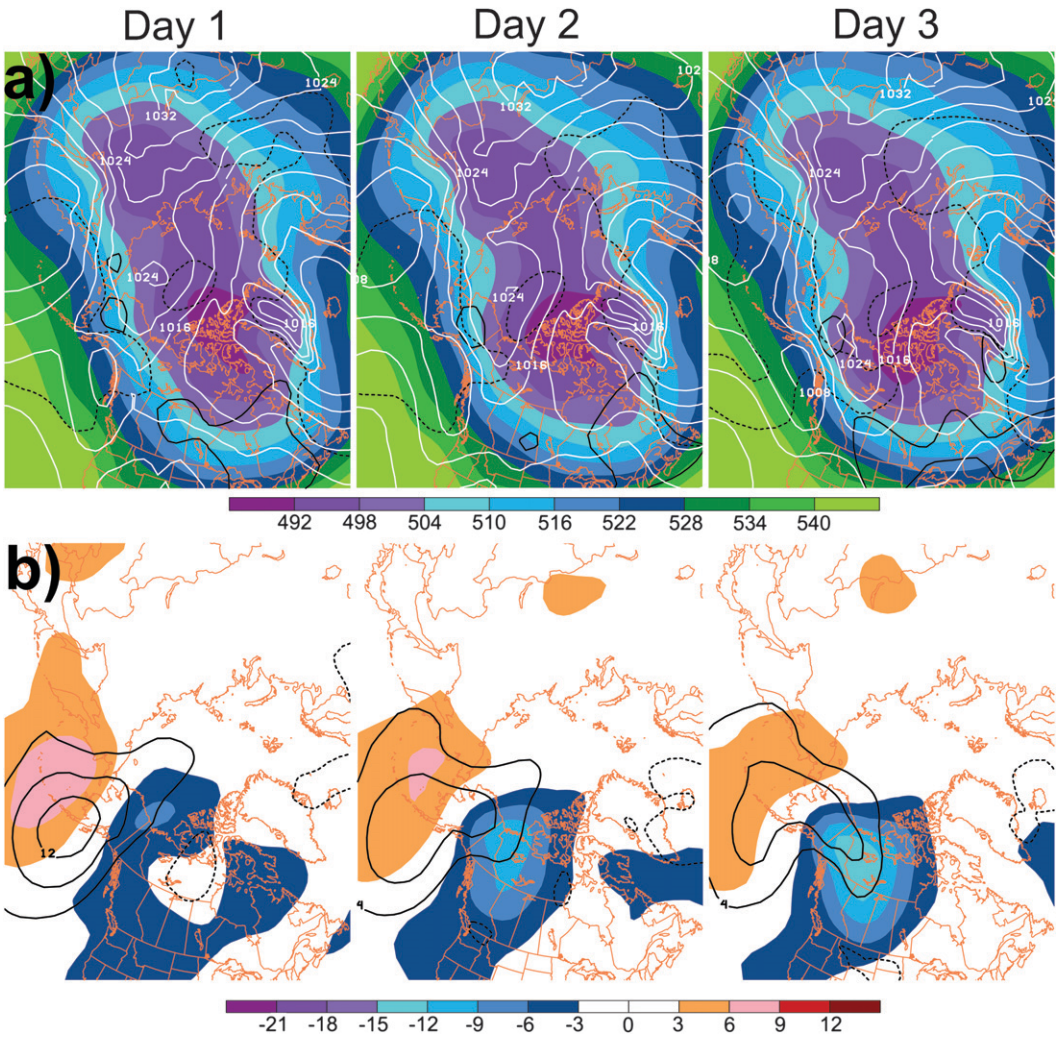

FIG. 4. (top) Daily (0600–0600 UTC) composites of the 53 mixed events' 1000–500-hPa thickness (dam) (shaded) and sea level pressure (white contours, every 4 hPa) for days 1–3 of the genesis period. Contours of 12-hPa standard deviation of sea level pressure (dashed) and 14-dam standard deviation of 1000–500-hPa thickness (black contours) are also shown. (bottom) 1000–500 thickness (dam) anomalies (shaded) and sea level pressure anomalies (contours, every 4 hPa) for days 1–3 of the genesis period. Anomalies are calculated relative to the 1948–2008 daily mean, not the running mean.

layer, advection and the residual term contribute almost equally to the cooling. However, the residual term dominates at lower levels. At the level closest to the surface, 1000 hPa, the mean and standard error of the residual contribution is -2.4 ± 0.9°C, -3.5 ± 0.5°C, and -0.8 ± 0.8°C for the deep, mixed, and shallow cases, respectively, whereas the contributions from cold-air advection are -1.8 ± 0.5°C, -1.8 ± 0.4°C, and -2.3 ± 0.6°C. It should be noted that for the shallow cases, 1000 hPa is likely to be above the temperature inversion. Although cold-air advection plays a role, the dominance of the residual term suggests that most of the intensification of the air mass is occurring locally.

As an indicator of cooling processes acting in the center of the air mass, the weather reports for days 1, 2, and 3 for deep, mixed, and shallow events at Norman Wells are given in Table 3. Snow is the most frequent report on the first day for all event types, 51% of observations during deep event genesis, 60% in mixed events, and 67% in shallow events. During the deep and mixed events, snow continues to be the most frequently reported on day 2, although the frequency decreases while reports of ice crystals and clear-sky increase. On day 3, ice crystals are the most frequent report. Ice crystals can cool layers above the surface and are reported most frequently in deep events and more frequently in

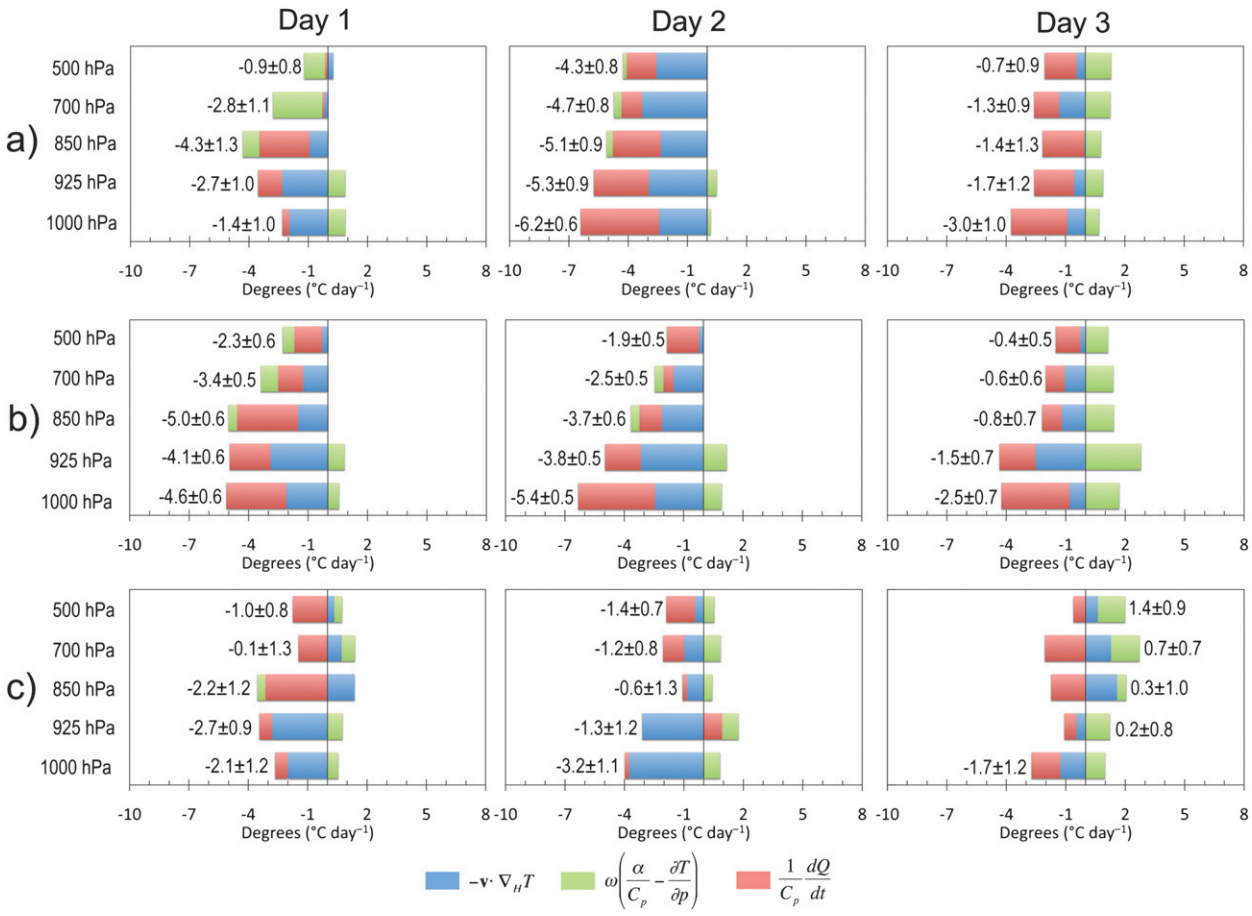

FIG. 5. Daily (0600–0600 UTC) change in temperature at the 1000-, 925-, 850-, 700-, and 500-hPa levels at Norman Wells from advection, vertical motion, and the residual for days 1–3 of the genesis period for (a) deep, (b) mixed, and (c) shallow events. There are 21 deep events, 53 mixed events, and 19 shallow events. The total change in temperature for a given day and pressure level is given next to the bars, ± the standard error, to the left for cooling and to the right for warming.

mixed events than in shallow events. During the shallow events, snow on the first day transitions to clear skies for the remainder of the genesis, consistent with high rates of surface cooling without tropospheric cooling.

The weather reports of snow, ice crystals, and ice fog in Table 3 show that these air masses contain condensate, with the exception being in the last two days of the shallow cases. Inside an air mass, the mixing ratio—the amount of water vapor in the air (g kg^{-1})—depends on temperature, since warmer air can contain more water vapor. However, the amount of condensate in the atmosphere depends on relative humidity, which is usually high in the events, even at low mixing ratios, owing to cold temperatures. The amount and location of condensate is a contributor to the rate and structure of the radiative cooling from ice crystals. A negative correlation exists between the daily change in temperature [the $\partial T/\partial t$ term of Eq. (1)] and the daily-averaged NCEP–NCAR reanalysis-derived mixing ratio at Norman Wells. The negative correlation indicates that moister days, as measured by the magnitude of the mixing ratio, are cooling faster—$\partial T/\partial t$ is negative and larger in magnitude—than drier days. The correlation coefficient at 850 hPa, typically the top of the moisture inversion, is −0.3 for all winter days, but greater, −0.5 (at 95% significance using a two-tailed Student's t test; Rahman 1968), considering only genesis days, implying that the relationship is stronger during arctic airmass formation. On nongenesis days, other processes, such as advection or vertical motion, may be a larger control of temperature change.

The weather reports in Table 3 also showed that the beginning of airmass genesis is characterized by snowfall. Besides increasing moisture in the subcloud layer, sublimation itself can contribute cooling. Evaporative cooling of rainfall is known to have an important effect in frontogenesis by increasing the rate of formation

TABLE 3. Hourly weather reports as a percentage of total reports at Norman Wells for days 1–3 for deep, mixed, and shallow event genesis. Most frequent observations on a given day are shown in bold type. There are 21 deep events, 53 mixed events, and 19 shallow events.

	Deep			Mixed			Shallow		
	Day 1	Day 2	Day 3	Day 1	Day 2	Day 3	Day 1	Day 2	Day 3
Clear/mostly clear	7	24	39	12	24	36	18	**37**	**46**
Cloudy/mostly cloudy	25	20	5	17	19	10	10	15	16
Ice crystals/ice fog	18	25	**41**	11	24	**39**	6	14	21
Snow/blowing snow	**51**	**30**	15	**60**	**34**	15	**67**	34	16

(Huang and Emanuel 1991; Katzfey and Ryan 1997; Oliver and Holzworth 1953). Fritsch et al. (1992) found that clouds and evaporative cooling enhance cold-air damming. Bell and Bosart (1988), in their paper on Appalachian cold-air damming, found that cold air masses could be formed on the lee side of the Appalachians by precipitation falling from aloft into a drier air layer and cooling the surface. Evaporative cooling accounted for 30% of the total cooling in these air masses. Sublimation of snow is also known to be a process for cooling a deep layer over a short period (Market et al. 2006) and is more efficient at cooling the atmosphere than rain at a given precipitation rate (Parker and Alan 1995).

A characteristic of cold-air damming, with an anticyclone in the lee of the mountains, was seen in Fig. 4. Observations of snow imply that, in addition to radiative processes, sublimation could be cooling the air mass. Since temperature changes owing to both radiative and latent heat processes are contained in the residual term, there is difficulty in determining their relative contribution. It could be inferred that if negative values of the residual term exist in unsaturated layers beneath a precipitating cloud, they are associated with sublimation cooling. Examining only genesis days when at least 80% of hourly weather reports were for either clear/mainly clear sky, snow/blowing snow, cloudy/mostly cloudy, or ice crystals/ice fog, the mean and standard error of the daily temperature change in the 1000 and 925 hPa layers (assumed to be subcloud) due to the residual term alone is -5.2 ± 1.3 for clear/mainly clear skies, -2.8 ± 0.8 for snow/blowing snow, 1.6 ± 2.9 for cloudy/mostly cloudy, and -1.8 ± 0.8 for ice crystals/ice fog. As an upper bound on the amount of cooling possible from sublimation at these temperatures, we calculate dT in the equation $C_p\, dT = -L_s\, dw$, where C_p is the specific heat of dry air at a constant pressure, T is the temperature in Celsius, L_s is the latent heat of sublimation, and w is the mixing ratio. Assuming the air temperature starts at −10°C, 1000 hPa, and 0% relative humidity, if snow sublimates into the air mass until reaching the saturation mixing ratio, the air will cool by 4.6°C.

Sublimation's effectiveness increases, as the subcloud layer's relative humidity decreases. As a check on the assumption that the 1000–925-hPa layer diabatic cooling during snowfall is sublimation cooling, the correlation coefficient between daily surface relative humidity and the subcloud diabatic term in that layer was calculated. The correlation is −0.3 (at 95% significance) during days with snow reports, meaning that the diabatic cooling is larger when humidity at the surface is lower. There is no statistically significant correlation between surface humidity and the diabatic term when snow is not reported.

We have seen that the arctic air masses are deep-layer phenomena that form in the presence of snow and ice fog. Soundings are useful to examine in detail the deep-layer vertical structure of the atmosphere. Since compositing soundings usually eliminates features of interest, the 1200 UTC soundings during the three genesis days at Norman Wells are presented for the same three events as in Fig. 3, in Fig. 6. During the deep case (Fig. 6a) the temperature decreases throughout the troposphere on all three days. From day 1 to the afternoon of day 2, snow was reported, changing to mainly cloudy at the end of day 2. The 850-hPa level is below the cloud deck, and at this level relative humidity increased by 14% while the temperature fell by 5°C. By day 3, no wind is reported at the surface and the weather is mainly clear sky with one report of ice crystals as an anticyclone in the region deepens. In the mixed case (Fig. 6b), heavy snow was also reported on day 1. Here, the 850-hPa level is in the cloud deck but below it, at 950 hPa, the relative humidity increases by 8% while the temperature decreases by 1.0°C. On day 3, clear skies are reported in the morning but by the afternoon thick ice fog reducing visibility to less than 2 km is reported. During the shallow case (Fig. 6c) there are clear skies and mostly clear skies reported over the period as the temperature falls to −40°C over the period. Uniquely in this case, there is warming above the 925 layer.

For all three examples the midtroposphere shows greater saturation on day 1 than on days 2–3 at the 700-hPa level in the deep case (Fig. 6a), from 1000–850 hPa in the

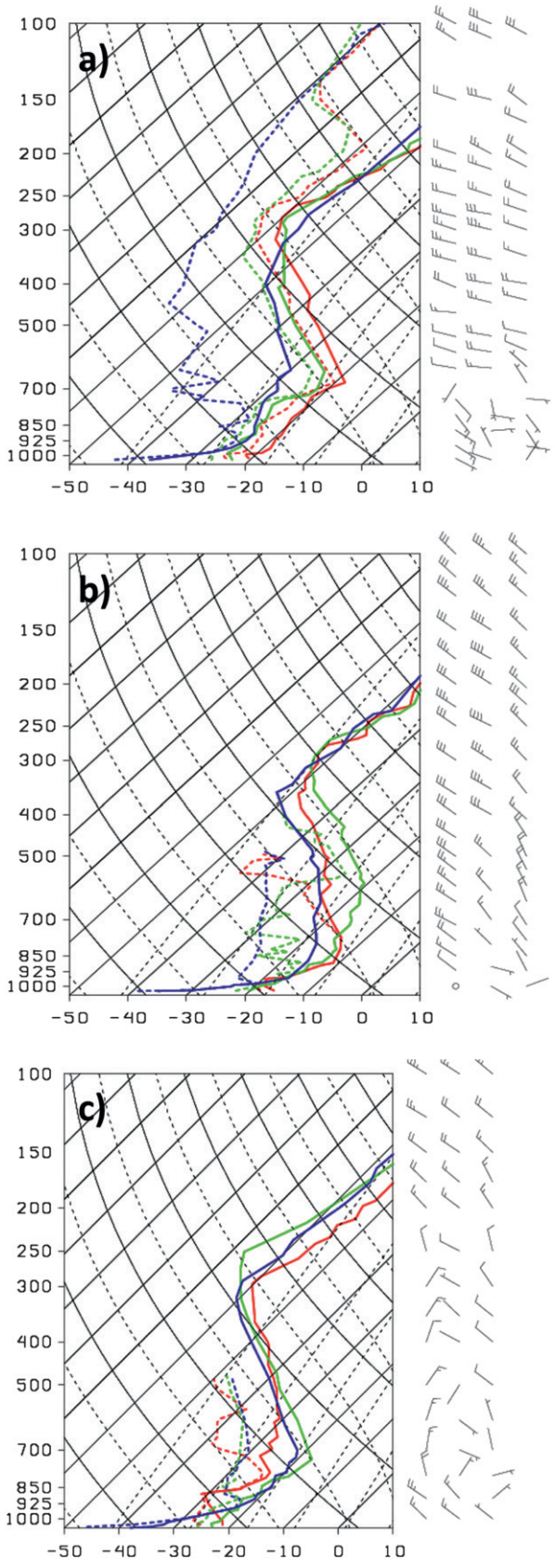

mixed case (Fig. 6b), and at 850 hPa in the shallow case (Fig. 6c). Over the same time period, saturation increases nearer the surface, most likely from sublimating snow rather than advection since the winds below 925 hPa are light, and also from falling temperatures. As the regional anticyclone intensifies and the atmosphere clears, there are dramatic surface temperature drops, creating temperature inversions.

A conceptualization of North American arctic airmass formation emerges as a deep-layer, multistage process. Greater snowfall amounts and cold-air advection are associated with deep events, clearer skies and more surface radiation cooling with shallow events. For all event types, the genesis typically begins with snowfall (Table 3) bringing moisture from aloft into the region, with ascent at above the 850-hPa level and descent in the 1000–925-hPa layer (Fig. 5). Some of the falling snow sublimates into the subcloud layers and there is radiative cloud-top cooling in upper layers. The freshly fallen snow layer has high emissivity. Therefore, as the sky clears, upwelling longwave surface radiation, with negligible incoming solar radiation, effects rapid surface temperature falls, as much as 18°C in one day. When the surface temperatures fall ice fog can form. The ice fog will insulate the surface, preventing further cooling there; however, the top of the fog cools radiatively, bringing the level of maximum cooling above the surface.

b. Maintenance and dissipation

The maintenance period lasts between 3 and 17 days with an average length of 6 days for deep events, 5 days for mixed events, and 4 days for shallow events (Table 2). Figure 7b shows the 1000–500-hPa thicknesses sea level pressure averaged over all days during the mixed-type events. Contours of 12-hPa standard deviation in sea level pressure (dashed, black), and contours of 14-dam standard deviation of thickness (solid, black) are also plotted. There is a 1024-hPa anticyclone oriented northwest to southeast, parallel to the Rockies, from Alaska and the Northwest Territories to southern Saskatchewan. Pressures of 1032 hPa are located on the Yukon–Northwest Territories border and in northern

←

FIG. 6. Temperature (solid) and dewpoint (dashed) soundings at Norman Wells for the 3 genesis days of a (a) deep, (b) mixed, and (c) shallow event. The genesis dates are 13–15 Feb 2003 for the deep event, 15–17 Dec 1989 for the mixed event, and 17–19 Dec 1980 for the shallow event. In all panels day 1 is plotted in red, day 2 in green, and day 3 in blue. Wind barbs (m s^{-1}) are plotted conventionally.

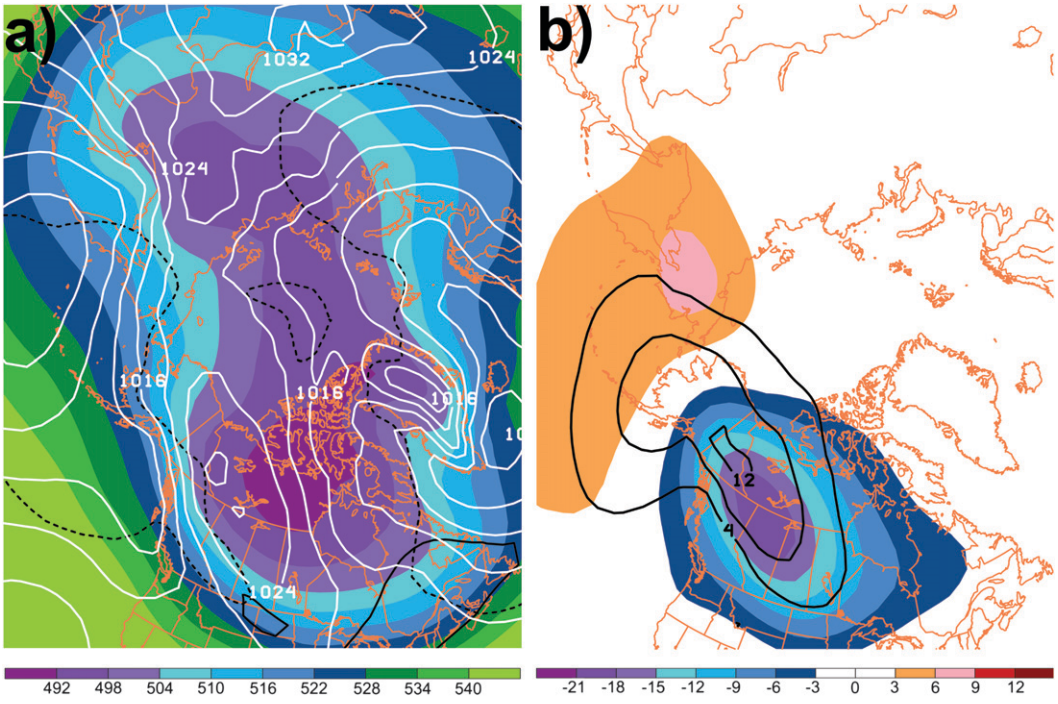

FIG. 7. (left) Composites of the mixed events daily (0600–0600 UTC) 1000–500-hPa thickness (dam) (shaded) and sea level pressure in hPa (contours, every 4 hPa). Contours of 12-hPa standard deviation of sea level pressure (dashed) and 14-dam standard deviation of 1000–500-hPa thickness (black contours) are also shown. (right) Composites of the mixed event daily 1000–500-thickness (dam) anomalies (shaded) and sea level pressure anomalies (contours, every 4 hPa for the maintenance period of mixed-type events. Anomalies are calculated relative to the 1948–2008 daily mean, not the running mean. There are 53 mixed-type events with an average length of 4.9 days, with a standard deviation of 2.4 days.

Alberta. Cold-air damming is still present, with an intense baroclinic zone along the mountains, separating warmer maritime air and the continental cold pool. Thicknesses as low as 492 dam are present over northern Canada.

Figure 7b, showing the composite 1000–500-hPa thickness and sea level pressure anomalies during the events, reveals anomalies of 12 hPa in the lee of the Mackenzie Mountains, connected to a broader region of high pressure anomalies in the North Pacific and Arctic Ocean. Cold thickness anomalies cover western Canada, with anomalies as low as −18–21 dam in northwestern Canada.

As with the genesis, the hourly weather reports as a percentage of total reports at Norman Wells for the deep, mixed, and shallow events were examined and are given in Table 4. The most common weather report in the deep and mixed cases is ice crystals/ice fog but there are also reports of clear skies. Clear sky is the most common weather type reported in the shallow cases, implying that shallow events tend to be drier. Although the latent heat contribution from ice crystals is zero—the condensation and evaporation of the crystals balance in general—they have a cooling effect through radiation that acts against the effect of subsidence. The percentage of snow reports are 8%, 19% lower than were found for the genesis period.

The averaged daily thermodynamic budgets during the events at Norman Wells (Fig. 8) show that there is a slight warming at all levels during the events themselves, with the exception of the 925-hPa level in the shallow composites. Although there is still cooling at all levels in the residual term, warming from subsidence overwhelms the cooling. This process weakens the strength of the anticyclone and the intensity of the surface temperature anomalies. Cold-air advection contributes less to the cooling than during the genesis, as

TABLE 4. Weather reports given as a percentage of total reports for that day at Norman Wells for deep, mixed, and shallow cases. Most frequent observations on a given day are bolded.

	Deep	Mixed	Shallow
Clear/mostly clear	27	33	**44**
Cloudy/mostly cloudy	11	6	10
Ice crystals/ice fog	**55**	**51**	27
Snow/blowing snow	8	11	20

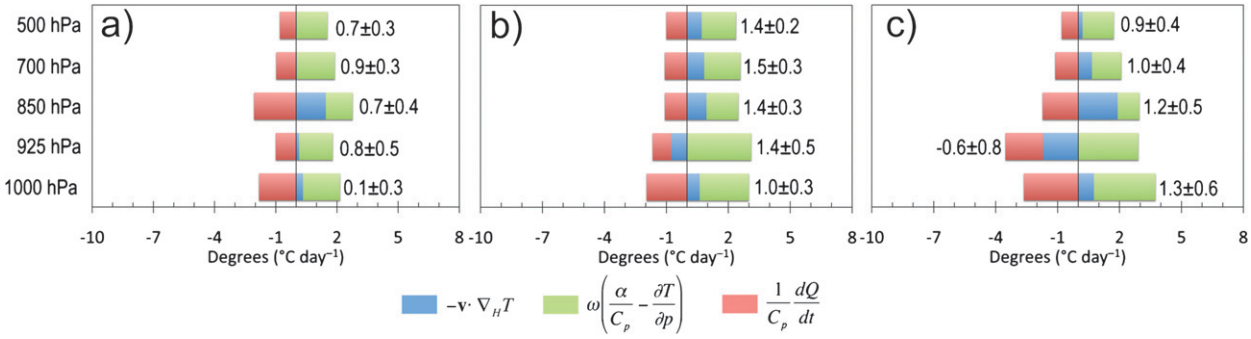

FIG. 8. Daily change in temperature averaged over all event days at the 1000-, 925-, 850-, 700-, and 500-hPa levels at Norman Wells due to the various thermodynamic terms for (a) deep events, (b) mixed events, and (c) shallow events. There are 21 deep events, 53 mixed events, and 19 shallow events. The total change in temperature for a given day and pressure level is written next to the bar, ± the standard error, to the left for cooling and to the right for warming.

at this time the anticyclone is well established with its associated low wind conditions.

There are several ways the arctic air masses eventually leave the area or dissipate. First, the air mass can be significantly weakened in situ by subsidence warming. Over the 5 days after an event, the daily mean surface temperature at Norman Wells warms on average, ± the standard error, by 7.7 ± 1.0°C. Figure 9 shows the average 1000–500-hPa thickness anomalies (shaded), relative to the 1948–2007 period, composited over the 5 days after all events, and the standard deviation of thickness anomalies (contours) during the same period. The average thickness fields show that the average track for air masses is eastward, over northern Quebec and into the North Atlantic. However, there are large values of thickness standard deviation, 14 dam, to the south of the average track, indicating high degrees of variability in this region; air masses occasionally flow southward, across the northern United States.

4. Secular change

The intensity of the events, measured by daily minimum surface temperature anomalies relative to a 30-year running mean, is not significantly changing in time, as shown in Table 2. However, the surface temperature itself during events is warming. Figure 10 is a histogram of all winter (DJF) minimum surface temperatures at the 10 stations used in this study (light shading) and the minimum surface temperatures during event days (dark shading), partitioned into the periods 1948–62, 1963–76, 1977–92, and 1993–2007. This partitioning divides the time series evenly into four 15-year periods. It can be seen in Fig. 10 that the temperature distribution at these stations has been shifting toward higher temperatures, both for the entire period and for the events. Temperatures below −50°C were observed in arctic air masses up until 1976 and not afterward, whereas temperatures as warm as −20°C were observed after 1993.

Under conditions of increased greenhouse gases, cooling from the emission of longwave radiation is partially offset by increased downwelling from the atmosphere. However, increased moisture and therefore ice crystal radiation in the midtroposphere during these events could compensate for decreased cooling at the surface. That the values of sublimation and radiative cooling in the air masses are both contained in the residual term complicates our understanding by combining the two mechanisms. Furthermore, owing to the extreme nature of these events, their infrequent occurrence makes statistically robust conclusions difficult. This section will explore possible secular changes in arctic airmass processes by examining trends in the depth of the cold pool,

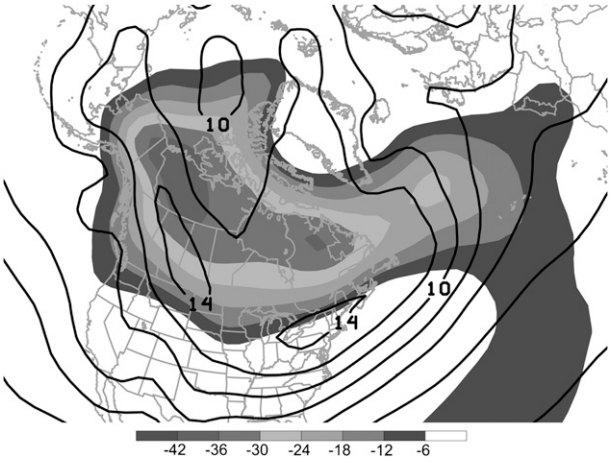

FIG. 9. Average 1000–500-hPa thickness anomalies (shaded, meters) and standard deviation of thickness anomalies (contours, dam) composited over 5 days following the events for all event types. Anomalies are calculated daily and are relative to the 1948–2007 average.

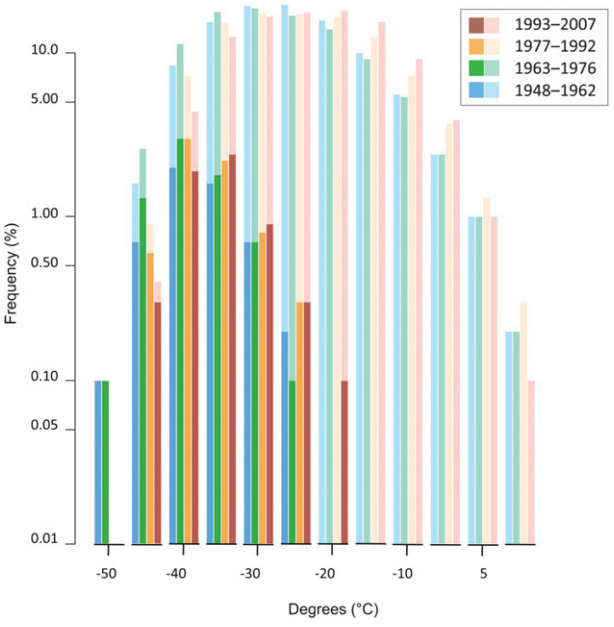

FIG. 10. Histogram of winter (DJF) daily minimum surface temperatures at the 10 stations used in this study for all days (pale shading) and event days (dark shading) for the periods 1948–62, 1963–76, 1977–92, and 1993–2007.

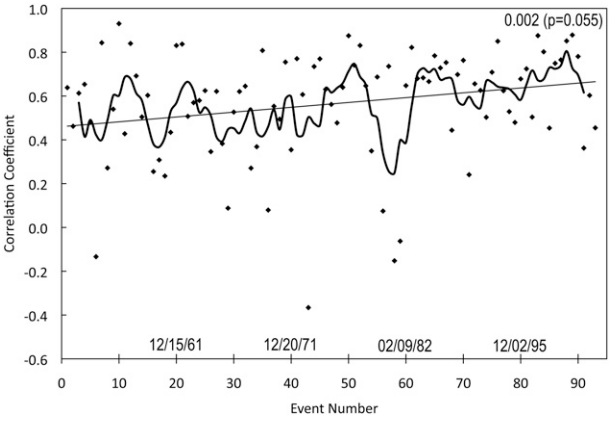

FIG. 11. Time series of correlation coefficients between daily surface minimum and 1000–500-hPa thickness for each event (points), the 5-event running mean (thick solid line), and the least squares regression trend of correlation coefficients (thin solid line). The trend (correlation coefficient per event) and p value are shown. The dates for the 20th, 40th, 60th, and 80th event are written on the horizontal axis for reference.

the contribution of thermodynamic terms to development, and maintenance and the moisture content of the air masses.

The time series of correlation coefficient between daily surface minimum temperature and 1000–500-hPa thickness for the 20 days leading up to and during events at Norman Wells is shown in Fig. 11. The trend of the correlation coefficient is toward increased correlation over time and is significant at the 95% level using a t test for significance. Therefore, the events are becoming deeper over time, consistent with the suggestion that there is increased likelihood of the presence of ice crystals in the later events, which act to bring the cooling to higher levels in the atmosphere.

Trends in the average magnitude of the thermodynamic terms at the 1000, 925, 850, 700, and 500 levels during the formation and maintenance of events were calculated by a least squares regression and summed over the 93 events to give a total change. The results are presented in Table 5. There are no significant trends during the genesis period; consistent with the finding that intensity relative to the mean has not changed (Table 2). The statistically significant changes are as follows: a decrease in 1000-hPa residual term cooling of 2.2°C day^{-1} and the 500-hPa temperature falls of 0.8°C day^{-1} during the maintenance period.

One possible explanation for decreased cooling in the residual term during the maintenance period is increased cloudiness, with downwelling radiation from clouds warming the surface and lower layers. Arctic and Antarctic clouds cause warming on balance at the surface through downwelling longwave radiation, rather than creating a net cooling effect due to their albedo as at lower latitudes (Intrieri et al. 2002; Town et al. 2005). Another possibility is the decreased effectiveness of ice crystals and ice fog at cooling the lower layers because of increased downwelling even in the absence of clouds, owing to increased greenhouse gas concentrations. It is difficult to quantify trends in cloudiness, density of ice crystals, or snowfall rates. Ice crystal density is not directly measured, although visibility measurements are available. However, at Norman Wells, we calculated no trend in the surface visibility.

The secular trends in relative humidity were examined during the maintenance period of the events using the NCEP–NCAR reanalysis at Norman Wells. The results at the 1000-, 850-, and 500-hPa layers are shown in Fig. 12, both for the relative humidity with respect to water (RH_{water}) and with respect to ice (RH_{ice}), both of which show similar behavior. RH_{ice} will primarily control the amount of cloudiness at upper levels and ice fog at lower levels during the winter at high latitudes, although as the temperature increases the likelihood of the presence of liquid water also increases. There is no trend in RH_{water} or RH_{ice} at the 500-hPa level and small trends, significant at the 95% level only for RH_{water} at 1000 hPa. There is a trend toward increased RH_{water} and RH_{ice} at 850 hPa, significant at 99%. Multiplying the slope of the trend by 93 events, RH_{ice} has increased by 17%. These calculations are complicated by a possible

TABLE 5. Total change over 93 arctic airmass events from 1948–2008 in thermodynamic terms for the (a) genesis period and (b) maintenance periods. Units are degrees Celsius day^{-1}. Bold typeface represents trends significant at 95%.

(a)	Temperature change	Horizontal advection	Vertical term	Residual
500	−0.2	1.0	−1.2	0.1
700	0.0	0.3	0.1	−0.4
850	−0.1	−0.3	0.4	−0.2
925	−0.7	−0.3	−0.8	0.4
1000	−0.2	0.2	−0.6	0.1
(b)	Temperature change	Horizontal advection	Vertical term	Residual
500	**0.8**	0.1	0.5	0.3
700	0.2	−0.8	0.3	0.6
850	0.2	0.7	0.2	−0.7
925	−0.2	−0.3	−0.8	0.9
1000	−0.1	−1.6	−0.7	**2.2**

discontinuity owing to changes in data assimilation in 1979 when satellite measurements become available. The statistical significance of the trends is eliminated when calculated separately over the periods 1948–78 and from 1979–2007.

There is also some evidence that snowfall during events is increasing. The average total snowfall at Norman Wells per event genesis and maintenance is given in Table 6. Compared to the snowfall per event averaged over 1948–92, the genesis average in 1993–2007 is statistically significant, using a two-tailed *t* test of means, at the 99% level for genesis and at the 95% level for the maintenance.

The increase in relative humidity at lower levels and the increase in snowfall indicate that the interior of the arctic air masses are becoming moister over time, particularly at the 850-hPa level (Fig. 12). Increased moisture at 850 hPa implies increased ice crystals at that level. This would act to decrease radiative cooling at the surface but increase radiative cooling at the top if the ice crystal layer, therefore increasing the height of the inversion. To some extent this is the behavior that has been observed, with increased depth of the events (Fig. 11), less diabatic cooling at the 1000-hPa level during events (Table 5) but increased diabatic cooling, although not statisticaly significant, at the 850-hPa level (Table 5).

5. Summary and conclusions

Arctic air masses were defined relative to a 30-year running mean to examine changes in their behavior independent of background changes in the mean temperature. Their formation takes place over several days. Temperatures begin to fall with a surface anticyclone present over northwestern Canada and a weak or absent Aleutian low. Snow falls into the developing air mass east of the Yukon Rocky Mountains over days 1 and 2 of the genesis increasing the moisture content of the lower levels. Cold-air advection and ascent in the upper atmosphere also contribute to the overall cooling.

During day 2, the temperature falls are most intense, especially at the 1000-hPa layer while the snowfall slows or abates. A lower-level temperature inversion forms and it becomes cold enough for ice crystals to condense out of the moistened air, creating ice fog. The top of the fog layer cools radiatively, creating more condensation of ice crystals at that point, deepening the fog. It was found that higher moisture levels in the 1000–850-hPa layer are correlated with more rapid temperature falls.

By day 3, the anticyclone has significantly intensified. The average surface pressure at Norman Wells during the event is 1028 ± 0.2 hPa. A strong baroclinic zone has formed along the mountains, with intense cold-air damming to their east. Subsidence is present throughout the 1000–500-hPa layer (Fig. 5). After the atmosphere clears, surface temperatures drop rapidly through radiative cooling. This multistage process for airmass formation is to our knowledge unique to the region as it combines cold-air damming in the lee of the Rocky Mountains and the extremely low temperatures typical of arctic latitudes that make ice crystals a common phenomenon there.

There is a high correlation between surface temperature and 1000–500-hPa thicknesses, indicating that cooling is taking place over a deep layer, contrary to the classical conception of an extremely shallow surface inversion. The depth of the inversion in the observations and the high correlation of the rate of cooling with moisture content are in strong agreement with the modeling study of Curry (1983). Furthermore, the correlation between surface temperature and the 1000–500-hPa thickness at Norman Wells has been increasing since 1948 (Fig. 11), indicating that the air masses are deepening over time. Surface temperatures have been warming but not relative to a running-mean temperature. An analysis

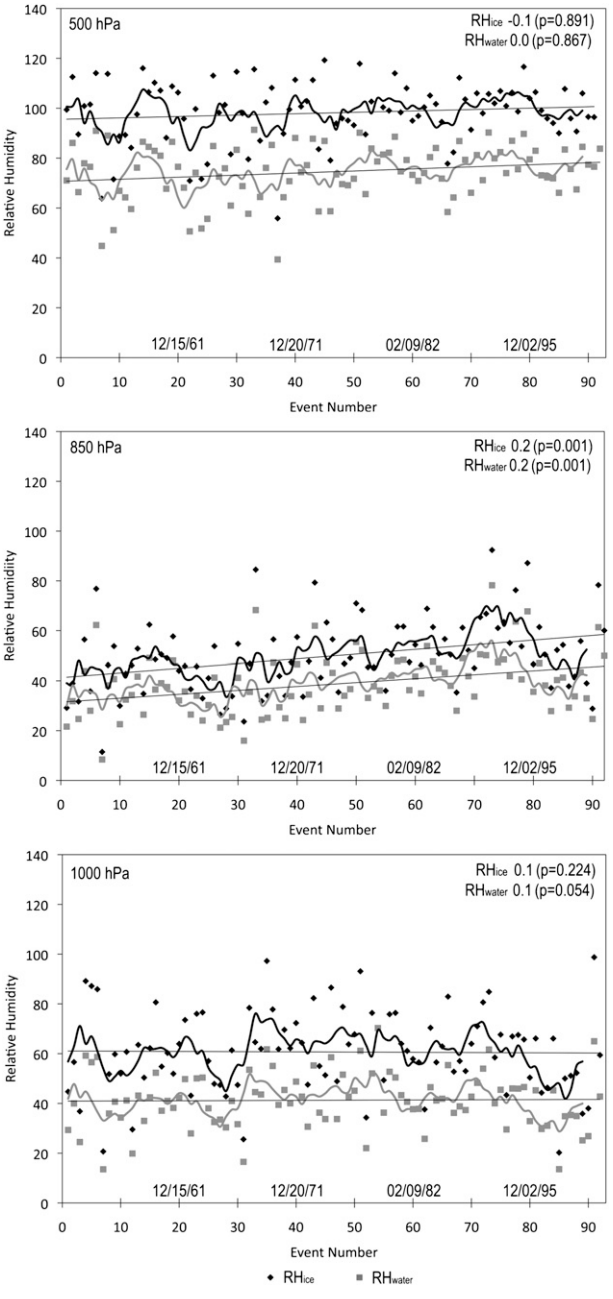

FIG. 12. Mean relative humidity over ice (black diamonds) and over water (gray squares) at Norman Wells for each of the 93 events from the NCEP–NCAR reanalysis, the 5-event running mean, and the least squares regression trends are also shown. The slope of the regression (percent event^{-1}) and its p values are given. The dates for the 20th, 40th, 60th, and 80th event are written on the horizontal axis for reference. The results for (top) 500, (middle) 850, and (bottom) 1000 hPa are shown.

of trends in the thermodynamic terms confirms this. There is no statistically significant trend in the daily temperature change during the genesis or maintenance phase of the events. However, during the event, the contribution of cooling from the residual term has decreased by 2.2°C day^{-1}, as calculated from a least squares regression over the 93 events.

TABLE 6. Average total snowfall per event with the 95% confidence interval for genesis and maintenance in 1948–62, 1963–76, 1977–92, and 1993–2007. The genesis period has been defined as lasting 3 days while the length of the maintenance period is at least 3 days but can be more; the average is 4 days.

	Genesis (cm)	Maintenance (cm)
1948–62	1.8 ± 1.0	1.3 ± 1.1
1963–76	2.0 ± 0.8	1.0 ± 0.7
1977–92	3.3 ± 1.9	1.1 ± 0.7
1993–2007	4.5 ± 1.8	2.6 ± 2.0

One possible explanation for the trend is increased cloudiness in the region. Snowfall during the airmass genesis has increased over time, as measured at Norman Wells, with a statistically significant increase to a mean value 4.5 ± 1.8 cm during formation in 1993–2007, compared to 1.8 ± 1.0 cm 1948–62. There is also a trend toward increased snowfall during event maintenance but of smaller magnitude than during formation (Table 6). RH_{ice} has been increasing during the events, by 17% at the 850-hPa level from 1948–2007 (Fig. 12) as calculated from a least squares regression over the 93 events.

Acknowledgments. The authors acknowledge Kerry Emanuel, and two anonymous reviewers, for their constructive comments. We would also like to thank Lucie Vincent at the Meteorological Service of Canada for providing the corrected daily temperature dataset. This research has been supported by a Natural Sciences and Engineering Research Council of Canada Discovery grant and International Polar Year Program grant.

REFERENCES

Bell, G. D., and L. F. Bosart, 1988: Appalachian cold air damming. *Mon. Wea. Rev.,* **116,** 137–161.

Bodurtha, F. T., 1952: An investigation of anticyclogenesis in Alaska. *J. Atmos. Sci.,* **9,** 118–125.

Brohan, P., J. J. Kennedy, I. Harris, S. F. B. Tett, and P. D. Jones, 2006: Uncertainty estimates in regional and global observed temperature changes: A new dataset from 1850. *J. Geophys. Res.,* **111,** D12106, doi:10.1029/2009JD011942.

Cellitti, M. P., J. E. Walsh, R. M. Rauber, and D. H. Portis, 2006: Extreme cold air outbreaks over the United States, the polar vortex, and the large-scale circulation. *J. Geophys. Res.,* **111,** D02114, doi:10.1029/2005JD006273.

Colucci, S. J., and J. C. Davenport, 1987: Rapid surface anticyclogenesis: Synoptic climatology and attendant large-scale circulation changes. *Mon. Wea. Rev.,* **115,** 822–836.

Curry, J., 1983: On the formation of continental polar air. *J. Atmos. Sci.,* **40,** 2278–2292.

——, 1987: The contribution of radiative cooling to the formation of cold-core anticyclones. *J. Atmos. Sci.,* **44,** 2575–2592.

——, F. G. Meyer, L. F. Radke, C. A. Brock, and E. E. Ebert, 1990: Occurrence and characteristics of lower-tropospheric ice crystals in the arctic. *Int. J. Climatol.,* **10,** 749–764.

Dallavalle, J. P., and L. F. Bosart, 1975: A synoptic investigation of anticyclogenesis accompanying North American polar air outbreaks. *Mon. Wea. Rev.,* **103,** 941–957.

Emanuel, K. A., 2009: Back to Norway: An essay. *Synoptic–Dynamic Meteorology and Weather Analysis Forecasting, Meteor. Monogr.,* No. 55, Amer. Meteor. Soc., 87–96.

Fritsch, J. M., J. Kapolka, and P. A. Hirschberg, 1992: The effects of subcloud-layer diabatic processes on cold air damming. *J. Atmos. Sci.,* **49,** 49–70.

Gotaas, Y., and C. S. Benson, 1965: The effect of suspended ice crystals on radiative cooling. *J. Appl. Meteor.,* **4,** 446–453.

Graversen, R. G., T. Mauritsen, M. Tjernstrom, E. Kallen, and G. Svensson, 2008: Vertical structure of recent Arctic warming. *Nature,* **451,** 53–56.

Huang, H.-C., and K. A. Emanuel, 1991: The effects of evaporation on frontal circulations. *J. Atmos. Sci.,* **48,** 619–628.

Intrieri, J. M., M. D. Shupe, T. Uttal, and B. J. McCarty, 2002: An annual cycle of Arctic cloud characteristics observed by radar and lidar at SHEBA. *J. Geophys. Res.,* **107,** 8030, doi:10.1029/2000JC000423.

Ioannidou, L., and P. M. K. Yau, 2008: Climatological analysis of the Mackenzie River basin anticyclones: Structure, evolution and interannual variability. *Atmospheric Dynamics,* M.-K. Woo, Ed., Vol. 1, *Cold Region Atmospheric and Hydrologic Studies: The Mackenzie GEWEX Experience,* Springer, 51–60.

Jones, P. D., and A. Moberg, 2003: Hemispheric and large-scale surface air temperature variations: An extensive revision and an update to 2001. *J. Climate,* **16,** 206–223.

Kalnay, E., and Coauthors, 1996: The NCEP/NCAR 40-Year Reanalysis Project. *Bull. Amer. Meteor. Soc.,* **77,** 437–471.

Katzfey, J. J., and B. F. Ryan, 1997: Modification of the thermodynamic structure of the lower troposphere by the evaporation of precipitation: A GEWEX cloud system study. *Mon. Wea. Rev.,* **125,** 1431–1446.

Konrad, C. E., and S. J. Colucci, 1989: An examination of extreme cold air outbreaks over eastern North America. *Mon. Wea. Rev.,* **117,** 2687–2700.

Market, P. S., R. W. Przybylinski, and S. M. Rochette, 2006: The role of sublimational cooling in a late-season Midwestern snow event. *Wea. Forecasting,* **21,** 364–382.

Oliver, V. J., and G. C. Holzworth, 1953: Some effects of the evaporation of widespread precipitation on the production of fronts and on changes in frontal slopes and motions. *Mon. Wea. Rev.,* **81,** 141–151.

Parker, D. J., and J. T. Alan, 1995: The role of snow sublimation in frontogenesis. *Quart. J. Roy. Meteor. Soc.,* **121,** 763–782.

Portis, D. H., M. P. Cellitti, W. L. Chapman, and J. E. Walsh, 2006: Low-frequency variability and evolution of North American cold air outbreaks. *Mon. Wea. Rev.,* **134,** 579–597.

Rahman, N. A., 1968: *A Course in Theoretical Statistics*. Charles Griffin and Company, 542 pp.

Shabbar, A., and B. Bonsal, 2003: An assessment of changes in winter cold and warm spells over Canada. *Nat. Hazards,* **29,** 173–188.

Smith, T. M., and R. W. Reynolds, 2005: A global merged land–air–sea surface temperature reconstruction based on historical observations (1880–1997). *J. Climate,* **18,** 2021–2036.

Tan, Y.-C., and J. A. Curry, 1993: A diagnostic study of the evolution of an intense North American anticyclone during winter 1989. *Mon. Wea. Rev.,* **121,** 961–975.

Town, M. S., V. P. Walden, and S. G. Warren, 2005: Spectral and broadband longwave downwelling radiative fluxes, cloud radiative forcing, and fractional cloud cover over the South Pole. *J. Climate,* **18,** 4235–4252.

Turner, J. K., and J. R. Gyakum, 2010: Trends in Canadian surface temperature variability in the context of climate change. *Atmos.–Ocean,* **48,** 147–162.

Vavrus, S., 2007: The role of terrestrial snow cover in the climate system. *Climate Dyn.,* **29,** 73–88.

Vincent, L. A., X. Zhang, B. R. Bonsal, and W. D. Hogg, 2002: Homogenization of daily temperatures over Canada. *J. Climate,* **15,** 1322–1334.

Vose, R. S., D. R. Easterling, and B. Gleason, 2005: Maximum and minimum temperature trends for the globe: An update through 2004. *Geophys. Res. Lett.,* **32,** L23822, doi:10.1029/2005GL024379.

Walsh, J. E., A. S. Phillips, D. H. Portis, and W. L. Chapman, 2001: Extreme cold outbreaks in the United States and Europe, 1948–99. *J. Climate,* **14,** 2642–2658.

Wexler, H., 1936: Cooling in the lower atmosphere and the structure of polar continental air. *Mon. Wea. Rev.,* **64,** 122–136.

——, 1937: Formation of polar anticyclones. *Mon. Wea. Rev.,* **65,** 229–236.

Zishka, K. M., and P. J. Smith, 1980: The climatology of cyclones and anticyclones over North America and surrounding ocean environs for January and July, 1950–77. *Mon. Wea. Rev.,* **108,** 387–401.